UMYU Scientifica, Vol. 4 NO. 3, September 2025, Pp 427 – 436
https://doi.org/10.56919/usci.2543.042
ISSN: 2955 – 1145 (print); 2955 – 1153 (online)
A periodical of the Faculty of Natural and Applied Sciences, UMYU, Katsina

ORIGINAL RESEARCH ARTICLE

Phytogenic Synthesis, Structural Elucidation and Antiplasmodial Activity of *Ocimum Gratissimum*-Mediated Silver Nanoparticles Against *Plasmodium Falciparum* Clinical Isolate

Auwal Ibrahim[1], Aminu Ado[3], Baba Gabi[1,2], Urwata M. Abdul-Azeez[1], Alhaji Umaru Bako[4] and Muktar Babagana[1]

[1]Department of Applied Chemistry, Kaduna Polytechnic, Kaduna, Nigeria
[2]Department of Biochemistry Kaduna State University, Kaduna, Nigeria
[3]Department of Microbiology, Federal University Dutsin-ma, Katsina State, Nigeria
[4]Department of Forestry Technology, Mohamet Lawan College of Agriculture, PMB 427, Maiduguri, Borno State, Nigeria

ABSTRACT

The growing resistance of *Plasmodium falciparum* to artemisinin-based combination therapies urgently calls for new antimalarial drugs. Silver nanoparticles (AgNPs) synthesized through green methods offer a promising therapeutic approach; however, research evaluating their efficacy against clinical parasite isolates and their direct comparison with standard antimalarial drugs remains limited. This study sought to biosynthesize and characterize AgNPs using *Ocimum gratissimum* L. leaf extract and to assess their antiplasmodial activity against clinical isolates of *P. falciparum*. AgNPs were synthesized by reacting a 1 mM silver nitrate ($AgNO_3$) solution with a 10% (v/v) aqueous leaf extract. The nanoparticles were characterized by UV-Vis spectroscopy, SEM, TEM, EDX, XRD, FTIR, DLS, and zeta potential analysis. Their *in vitro* antiplasmodial efficacy was evaluated against clinical *P. falciparum* strains using a 48-hour schizont inhibition assay. The half-maximal inhibitory concentration (IC_{50}) was calculated via probit regression and directly compared to that of quinine. The optimized protocol produced spherical, crystalline AgNPs with a core size of 42.5 ± 5.2 nm (by TEM), a hydrodynamic diameter of 58.3 ± 8.1 nm, and a zeta potential of -28.7 ± 2.1 mV, confirming excellent colloidal stability. FTIR analysis verified the role of plant phytochemicals in reducing and capping the nanoparticles. The *O. gratissimum*-AgNPs demonstrated significant, dose-dependent antiplasmodial activity, reaching 76.68 ± 1.44% inhibition at 100 µg/mL. The IC_{50} value was determined to be 13.70 ± 0.99 µg/mL, indicating moderate potency relative to quinine (IC_{50} = 3.14 ± 0.74 µg/mL). This work successfully establishes *O. gratissimum* as a viable source for producing stable AgNPs with substantial efficacy against drug-resistant clinical malaria parasites. The direct, quantitative comparison with quinine and the comprehensive analysis linking physicochemical properties to biological activity provide a solid foundation for future antimalarial nanotherapeutic development. Significance Statement: These findings validate a green nanotechnology strategy that utilizes local medicinal plants, presenting a potent, stable, and sustainable candidate for use as an adjunct in combination therapy against drug-resistant malaria.

ARTICLE HISTORY

Received June 24, 2025
Accepted September 19, 2025
Published September 30, 2025

KEYWORDS

Phytogenic, *Ocimum gratissimum*, Silver Nanoparticles, Quinine, Anti-plasmodial and *P. falciparum*

INTRODUCTION

Malaria persists as one of the world's most severe infectious diseases, with a disproportionate impact in sub-Saharan Africa. *Plasmodium falciparum* is the primary cause, responsible for the majority of the 247 million estimated annual cases and over 600,000 deaths (WHO, 2023; Shahzadi et al., 2025). The relentless emergence and spread of *resistant* strains to conventional and first-line artemisinin-based combination therapies (ACTs) highlight an urgent and unmet need for novel therapeutic agents with distinct mechanisms of action (Rathod et al., 2021; Fatima, 2024). In this context, green nanotechnology the synthesis of metal nanoparticles using biological sources has emerged as a promising strategy for developing new antiparasitic formulations (Iravani, 2011; Barati et al., 2024). Plant-mediated synthesis of silver nanoparticles (AgNPs) is particularly advantageous, as it combines the innate bio-reductive potential of phytochemicals with the unique physicochemical properties of nanomaterials, such as enhanced surface area, targeted delivery potential, and improved bioavailability (Ahmed et al., 2016; Rai et al.,

Correspondence: Auwal Ibrahim. Department of Applied Chemistry, Kaduna Polytechnic, Kaduna, Kaduna State, Nigeria. ✉ iauwal790@gmail.com.

How to cite: Ibrahim, A., Ado, A., Gabi, B., Abdul-Azeez, U. M., Bako, A. U., & Babagana, M. (2025). Phytogenic Synthesis, Structural Elucidation and Antiplasmodial Activity of *Ocimum Gratissimum*-Mediated Silver Nanoparticles Against *Plasmodium Falciparum* Clinical Isolate. *UMYU Scientifica*, 4(3), 427 – 436. https://doi.org/10.56919/usci.2543.042

2021). The resulting "nanobio-hybrid" structures often exhibit synergistic activity superior to that of crude plant extracts or chemically synthesized counterparts (Karthik et al., 2022; Singh et al., 2024; Sharma et al., 2024). Among various medicinal plants, species of the *Ocimum* genus are frequently employed due to their well-documented phytochemical richness. For instance, several studies have reported the synthesis of AgNPs using *O. basilicum*, *O. sanctum*, and *O. gratissimum* for antimicrobial and antioxidant applications (Mela Yoro et al., 2022; Lawal et al., 2024).

However, a critical analysis of the literature reveals a significant research gap. While the antiplasmodial potential of AgNPs is gaining recognition, studies specifically targeting *clinical isolates* of *P. falciparum* with plant-based AgNPs remain relatively scarce. Furthermore, existing reports on *O. gratissimum*-AgNPs have primarily focused on their antibacterial properties (Banerjee et al., 2024; Egwu et al., 2024), demonstrating a pronounced lack of comprehensive antiplasmodial profiling against drug-resistant clinical isolates, direct and quantitative comparison of efficacy with standard antimalarial drugs like quinine, and rigorous structural-activity correlation linking detailed physicochemical characterization (zeta potential, crystallite size) to the observed biological activity. This study specifically addresses these gaps by selecting *Ocimum gratissimum* L. not merely for its generic phytochemical profile, but for its established ethnobotanical use in fever management and the documented presence of potent secondary metabolites like eugenol, thymol, and rosmarinic acid, which possess intrinsic antiplasmodial properties (Ibrahim & Musa, 2022). We hypothesize that these specific compounds will not only mediate the reduction of Ag^+ ions but also form a synergistic bioactive cap on the nanoparticle surface, thereby enhancing antiplasmodial efficacy. The novelty of this work is therefore multi-faceted. It systematically evaluates the antiplasmodial activity of *O. gratissimum*-AgNPs against a *clinical isolate* of *P. falciparum* for a therapeutically relevant assessment, establishes a direct quantitative comparison of their IC_{50} with the standard drug quinine to contextualize potency, and provides a deepened analytical rationale by correlating a full suite of characterization data (including DLS, zeta potential, and XRD) with the biological outcome. Therefore, this study aims to synthesize AgNPs using a Nigerian cultivar of *O. gratissimum*, to characterize them with advanced analytical techniques, and to rigorously evaluate their *in vitro* antiplasmodial activity. The ultimate goal is to determine whether this green nanotherapeutic platform can yield a potent, stable, and locally sourced adjunct for malaria therapy, thereby contributing a validated and translatable approach to the nanomedicine arsenal against drug-resistant malaria

MATERIALS AND METHODS

Plant material and standardized aqueous extraction

Fresh leaves of *Ocimum gratissimum* were collected, authenticated (voucher no. KASU/BS/313) and air-dried in the shade for 10–14 days. Dried material was milled to a fine powder. For each extraction, 20.0 g of leaf powder was mixed with 100 mL of distilled water (plant:solvent ratio 1:5 w/v) and heated at 60 ± 2 °C for 30 minutes with continuous magnetic stirring. The extract was cooled to room temperature, filtered through Whatman No. 1 filter paper, and centrifuged at 4,000 × g for 10 min to remove particulates. The clarified extract was aliquoted and stored at 4 °C (maximum 3 days) before use. All extraction steps were performed in triplicate (independent biological replicates) to ensure reproducibility.

Green synthesis of silver nanoparticles (O. gratissimum–AgNPs)

1.0 mM silver nitrate ($AgNO_3$) stock solution was freshly prepared in deionized water. For synthesis, 90 mL of 1.0 mM $AgNO_3$ was mixed with 10 mL of the aqueous *O. gratissimum* extract (final volume 100 mL; $AgNO_3$:extract ratio 9:1 v/v). The reaction mixture was stirred at room temperature (23–25 °C) and monitored for colour change (pale yellow → brown) as an initial indicator of Ag^+ reduction. The mixture was kept under stirring for 24 h to ensure completion of reduction. The colloidal suspension was centrifuged at 10,000 rpm (≈10,000 × g) for 15 minutes; the pellet was washed three times with deionized water and once with ethanol to remove unbound phytochemicals, then dried in a vacuum oven at 40 °C and stored in amber vials at 4 °C. Final AgNP stock concentrations were prepared at 1 $mg \cdot mL^{-1}$ in sterile deionized water and sonicated 10 min immediately before bioassays to ensure dispersion. All syntheses were performed in at least three independent batches ($n \geq 3$ biological replicates).

Hydrodynamic size and zeta potential: Measured by dynamic light scattering (DLS) in triplicate to evaluate colloidal stability.

Characterization of Synthesized AgNPs

The synthesized AgNPs were characterized using the following techniques:

Fourier Transform Infrared Spectroscopy (FTIR)

The functional groups responsible for the reduction and capping of AgNPs were identified using an FTIR spectrometer (Perkin Elmer Inc., USA) in the attenuation total reflectance (ATR) mode. Spectra were recorded in the range of 4000–400 cm^{-1} (Salisu *et al.*, 2022, 2019, 2020, 2024).

Scanning Electron Microscopy (SEM) and Energy Dispersive X-ray Spectroscopy (EDX)

The surface morphology and elemental composition of the AgNPs were analyzed using SEM (JEOL JSM-IT200) Japan coupled with an EDX detector. The sample was sputter-coated with a thin layer of gold prior to imaging to enhance conductivity.

Transmission Electron Microscopy (TEM)

The particle size distribution and shape were determined using TEM (JEOL JEM-1400) Japan. A drop of the

sonicated AgNP suspension was placed on a carbon-coated copper grid and allowed to dry before analysis. The size of over 200 nanoparticles from multiple TEM images was measured using ImageJ software to determine the average size and distribution.

X-ray Diffraction (XRD)

The crystalline structure was analyzed using an X-ray diffractometer (Bruker D8 Advance) with Cu Kα radiation (λ = 1.5406 Å). The scanning rate was 0.02°/s over a 2θ range of 20° to 80°. The average crystallite size (D) was calculated from the full width at half maximum (FWHM, β) of the most intense peak using the Debye-Scherrer equation:

$$D = K\lambda / (\beta \cos\theta)$$

where K is the shape factor (0.9), λ is the X-ray wavelength, β is the FWHM in radians, and θ is the Bragg angle.

Preparation of test solutions for bioassays

Stock suspensions (1 mg·mL^{-1}) were prepared in sterile deionized water, sonicated for 10 min and filter-sterilised through a 0.22 μm syringe filter where feasible. Working concentrations were prepared by serial dilution in complete culture medium to yield a final concentration range of 1.54 to 100 μg·mL^{-1} (matching the range used in this study). Vehicle controls (equivalent volume of sterile water) and positive controls (quinine; serial dilutions prepared fresh) were included in every assay plate.

Parasite, RBC sourcing and ethical considerations

Clinical isolates of *Plasmodium falciparum* were obtained from consenting malaria patients following institutional ethical approval (Ethics Committee reference: MOH/ADM/744/VOL.1/459. Human O^+ erythrocytes were sourced from healthy screened donors at Barau Dikko Teaching Hospital Kaduna, Nigeria, screened for transfusion-transmissible infections (HIV, HBV, HCV, syphilis) and used within 7 days of collection. All human sample collection followed the local institutional guidelines; written informed consent was obtained from donors.

In vitro parasite culture conditions

Parasites were cultured using standard procedures with minor modifications:

Medium: RPMI 1640 supplemented with 25 mM HEPES, 0.2% sodium bicarbonate, 50 μg·mL^{-1} hypoxanthine, 25 μg·mL^{-1} gentamicin and 10% heat-inactivated human AB serum.

Hematocrit and parasitemia: Cultures maintained at 2% hematocrit. For antiplasmodial assays, synchronous ring-stage cultures were adjusted to an initial parasitemia of 1.0–2.0% (measured by thin smear) to ensure exponential growth during the assay period. Cultures incubated at 37.0 ± 0.5 °C in a controlled atmosphere of 5% CO_2, 5% O_2 and 90% N_2 (tri-gas incubator) or a candle-jar setup achieving similar conditions. Parasite populations were synchronized to ring stage using 5% D-sorbitol treatment (2% v/v sorbitol in water) according to Lambros & Vanderberg (1979) protocol: sorbitol treatment for 10 min at 37 °C, followed by two washes with RPMI and resuspension. Synchronization was performed twice, 48 h apart, when tighter synchrony was required. Synchronization efficiency was confirmed by microscopic examination (≥90% ring stages before assay).

In vitro antiplasmodial assay (schizont inhibition)

Antiplasmodial activity was assessed using a standard 48-hour schizont inhibition assay with modifications: Synchronized ring-stage cultures (1–2% parasitemia; 2% hematocrit) were dispensed into 96-well flat-bottom plates (200 μL per well). Test samples (AgNPs) were added at final concentrations of 1.54, 3.13, 6.25, 12.5, 25, 50 and 100 μg·mL^{-1}. Each concentration was run in technical triplicate wells. Each independent biological experiment (n ≥ 3) used fresh parasite cultures and independently prepared AgNP suspensions. Controls: positive control quinine (same concentration range), vehicle control (sterile water), and untreated control were included on each plate. Plates were incubated for 48 h. At the endpoint, thin blood smears were prepared from each well, air-dried, methanol-fixed and stained with 10% Giemsa for 15 minutes. Parasitemia and stage distribution were determined by counting ≥2,000 erythrocytes per slide under oil immersion (100× objective). Schizont counts were quantified and percent inhibition relative to untreated control calculated using:

%Parasite Viability = (Parasitemia in Test Well / Parasitemia in Negative Control Well) × 100

% Schizont Inhibition = [(Schizont Count in Control - Schizont Count in Test) / Schizont Count in Control] × 100

Determination of IC_{50}

IC_{50} values (concentration giving 50% inhibition) were estimated by probit regression of the concentration–response data. Prior to probit analysis, concentrations were $\log_{10}$-transformed. Probit regression assumptions and checks included: Linearity (in probit space) of the dose–response relationship after log-transformation; Independent observations (biological replicates treated independently); Homogeneity of variance across dose groups (checked visually and via tests); Adequate goodness-of-fit assessed by deviance statistics and inspection of residuals.

IC_{50} estimates are reported with 95% confidence intervals (CIs). Where appropriate, IC_{50}s from individual biological replicates were pooled using a mixed-effects model

Statistical analysis

All experiments were performed as ≥3 independent biological replicates, each with technical triplicates. Data

are presented as mean ± standard deviation (SD) for biological replicates. For clarity, mean ± standard error of the mean (SEM) may be used for graphical presentation where noted; the text reports SD and the number of biological replicates (n). Each dataset was tested for normality using the Shapiro–Wilk test. Homogeneity of variance: Assessed using Levene's test. One-way ANOVA was used when comparing multiple concentrations of a single factor, assuming data met normality and homoscedasticity. Where ANOVA indicated significance ($p < 0.05$), pairwise post hoc comparisons were performed using Dunnett's test (comparing treatments vs control). Probit regression, performed on log_{10}-transformed concentration–response data to estimate IC_{50} and 95% CIs. Goodness of fit and residual plots were evaluated; Statistical analyses and curve fitting were performed using GraphPad Prism (version 9.x), SPSS (version 26). A two-tailed $p < 0.05$ was considered statistically significant.

RESULTS

Elemental analysis using EDX (Figure 2; Table 2) showed silver as the major component (49.26% by weight; 11.09% atomic concentration), alongside carbon (70.47% atomic), nitrogen (10.64%), and trace elements including Si, Al, Mg, Fe, Cl, K, Na, S, P, Ca, and Ti. The presence of these elements suggests phytochemical capping, which enhances nanoparticle stability and biocompatibility. TEM micrographs (Figure 3) further showed that the nanoparticles were well dispersed with minimal aggregation, suggesting effective capping by plant biomolecules. XRD analysis (Figure 4) confirmed the crystalline nature of the AgNPs, displaying distinct diffraction peaks characteristic of a face-centered cubic silver structure.

FTIR spectra (Table 3; Figure 4) exhibited major absorption bands at 2952.1 cm^{-1} (C–H stretching), 1796.6 cm^{-1} (C=O stretching from aldehyde and ester groups), and 1899.7 cm^{-1} (aromatic NO_2 stretching), indicating the involvement of biomolecules in both reduction and stabilization. The synthesized AgNPs exhibited significant, concentration-dependent *in vitro* antiplasmodial activity against clinical strains of *Plasmodium falciparum*. As shown in Table 5, inhibition increased progressively from 6.68 ± 1.44% at 1.54 µg/mL to 76.68 ± 1.44% at 100 µg/mL. Correspondingly, parasite viability decreased with increasing concentrations, reflecting impaired schizont development (Figure 6).

Comparative analysis with quinine (Figures 7 and 8) revealed that quinine achieved 93.79 ± 0.55% inhibition at 100 µg/mL, *O. gratissimum*-AgNPs displayed substantial inhibitory effects with an IC_{50} of 13.70 ± 0.99 µg/mL, compared to 3.14 ± 0.74 µg/mL for quinine.

Table 1: Optimization of Synthesis Parameters for *O. gratissimum*-AgNPs

Parameter	Range Tested	Optimal Condition	Observed Effect
Extract Concentration	5% - 20% (v/v)	10%	Lower concentrations led to incomplete reduction; higher concentrations caused rapid aggregation.
pH	5 - 10	8.0	Neutral to slightly basic pH favored smaller, more uniform nanoparticles.
Reaction Temperature	25°C - 80°C	25°C (Room Temp.)	Efficient synthesis at ambient temperature underscores the energy-efficient nature of the process.
Reaction Time	10min-24H	24 H	Color stabilization and UV-Vis peak narrowing indicated completion after 24 hrs.

Table 2: Elemental Composition of The Synthesised *Ocimum gratissimum -AgNPs*

Element Number	Element Symbol	Element Name	Atomic Conc. (%)	Weight Conc. (%)
47	Ag	Silver	11.09	49.26
6	C	Carbon	70.47	34.85
7	N	Nitrogen	10.64	6.14
14	Si	Silicon	1.68	1.94
13	Al	Aluminium	1.47	1.64
12	Mg	Magnesium	1.32	1.32
26	Fe	Iron	0.46	1.06
17	Cl	Chlorine	0.60	0.88
19	K	Potassium	0.47	0.76
11	Na	Sodium	0.67	0.64
16	S	Sulfur	0.46	0.60
15	P	Phosphorus	0.44	0.56
20	Ca	Calcium	0.22	0.36
22	Ti	Titanium	0.00	0.00

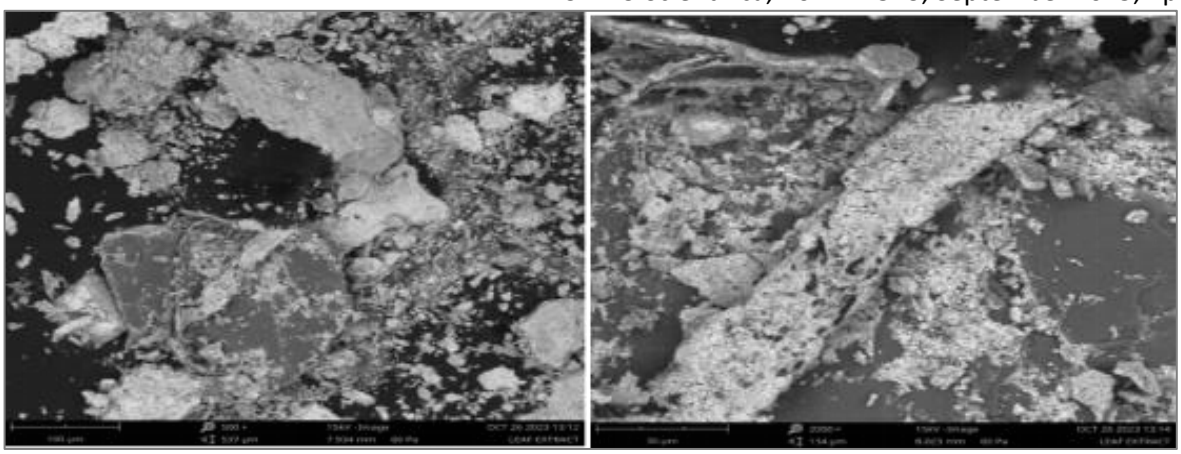

Figure 1: Show the SEM Image of the Green synthesized *Ocimum gratissimum* -AgNPs

Figure 2: EDX spectra of Green synthesized *Ocimum gratissimum* -AgNPs

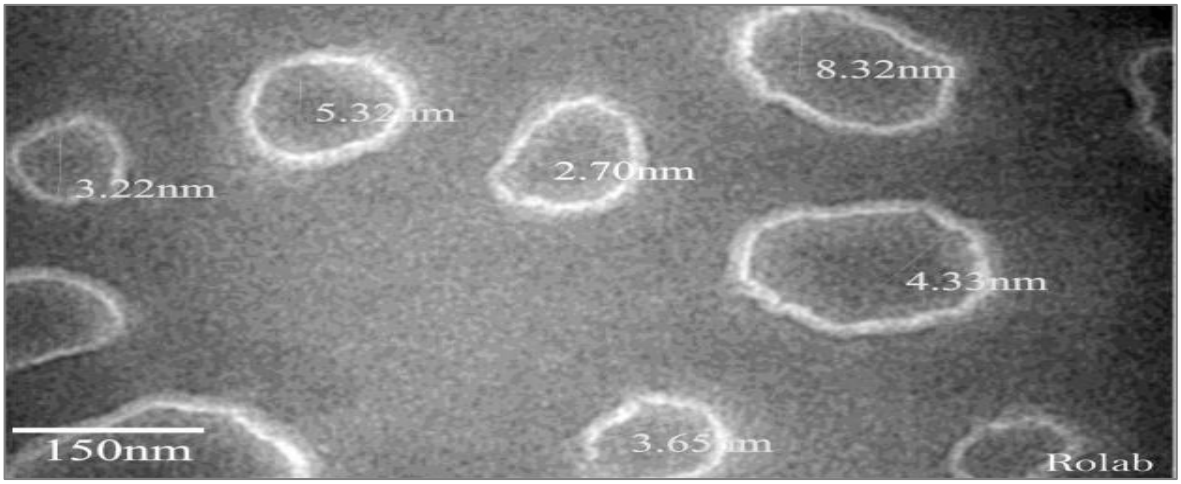

Figure 3: Show the TEM Image of Particle size distribution of the Green Synthesized *Ocimum gratissimum*-AgNPs

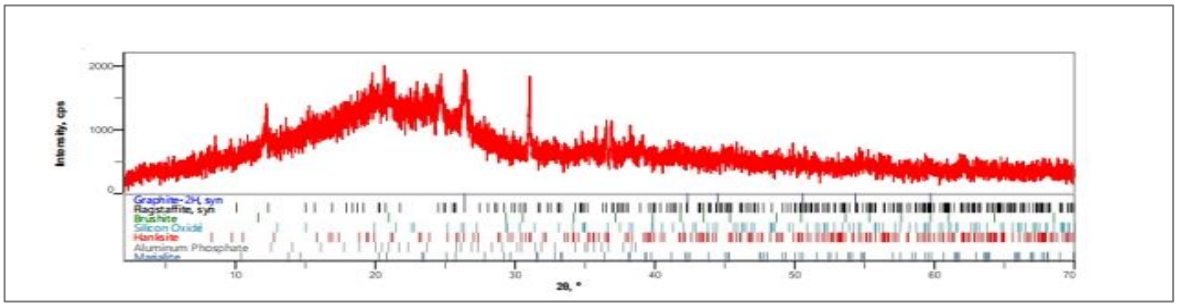

Figure 4: XRD Spectrum of the Green synthesized *O. gratissimum* -AgNPs

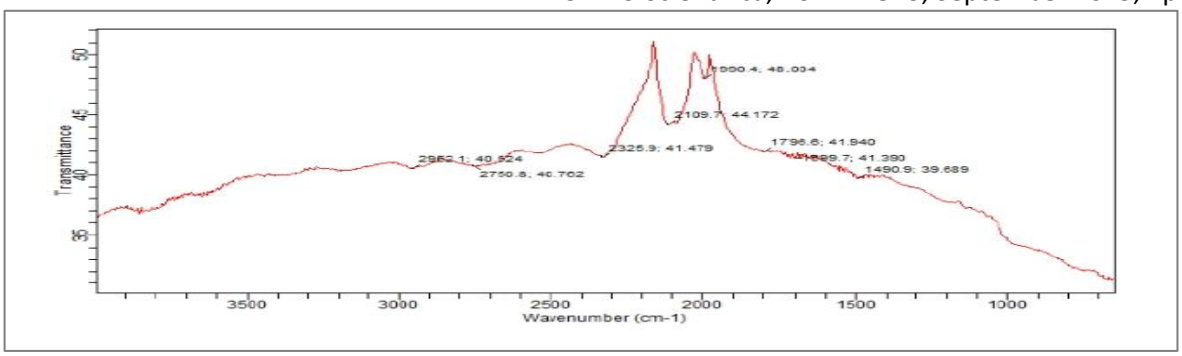

Figure 5: IR Spectrum of the Green synthesized Ocimum gratissimum -AgNPs

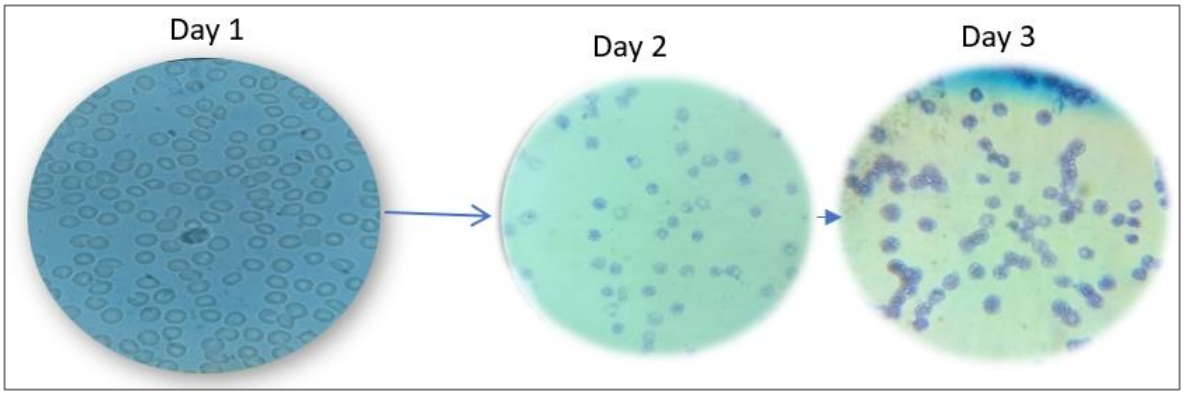

Multiple Trophozoite Multiple Schizonts

Figure 6: The Microscopic View of *In vitro* Culture of Asexual stage of *Plasmodium falciparum* Clinical strain

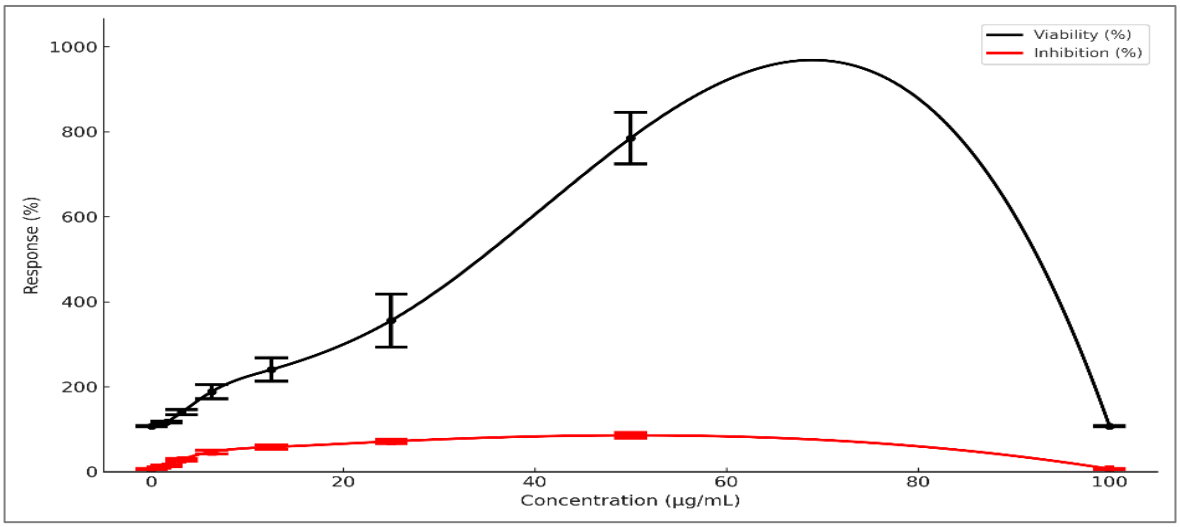

Figure 7: Dose-dependent viability and inhibition of Plasmodium falciparum exposed to *O. gratissimum*–AgNPs.

Table 3: Detailed FTIR Functional Group Assignments for *O. gratissimum*-AgNPs

Wave Number (cm^{-1})	Vibrational Mode	Functional Group	Proposed Biomolecule Role
3280 (broad)	O-H Stretching	Phenols, Alcohols	Stabilization via H-bonding; major reducing agents.
2952.1	C-H Stretching	Alkanes (Methylene)	From fatty acid chains or terpene skeletons.
1796.6	C=O Stretching	Aldehydes, Esters	Aldehyde group oxidation to carboxylic acid is a key reduction mechanism.
1650.4	C=O Stretching	Amide I (Proteins)	Proteins strongly involved in capping and stabilization.
1458.2	N=O Stretching	Nitro Compounds (Aromatic)	Specific to certain secondary metabolites; may contribute to bioactivity.
1075.5	C-O-C Stretching	Polysaccharides	Indicates involvement of flavonoids or polysaccharides in stabilization.

Table 4: Summary of Physicochemical Characteristics of *O. gratissimum*-AgNPs

Characterization Technique	Key Result	Interpretation
UV-Vis Spectroscopy	λ~max~ = 428 nm	Confirms Surface Plasmon Resonance (SPR), indicating spherical AgNP formation.
SEM/TEM	Spherical, Well-dispersed	Anisotropic shape due to uniform phytochemical capping; minimal aggregation.
TEM Size Distribution	42.5 ± 5.2 nm	Precise measurement of the metallic core diameter.
DLS (Hydrodynamic Size)	58.3 ± 8.1 nm	Larger size than TEM confirms the presence of the phytochemical capping layer in solution.
Polydispersity Index (PDI)	0.19	Indicates a moderately monodisperse population (PDI < 0.2).
Zeta Potential	-28.7 ± 2.1 mV	High negative surface charge ensures excellent colloidal stability by electrostatic repulsion.
XRD	FCC Crystalline Structure	Confirms metallic silver with high crystallinity; no impurity phases detected.
EDX	Strong Ag signal at ~3 keV	Verifies elemental silver as the primary component.

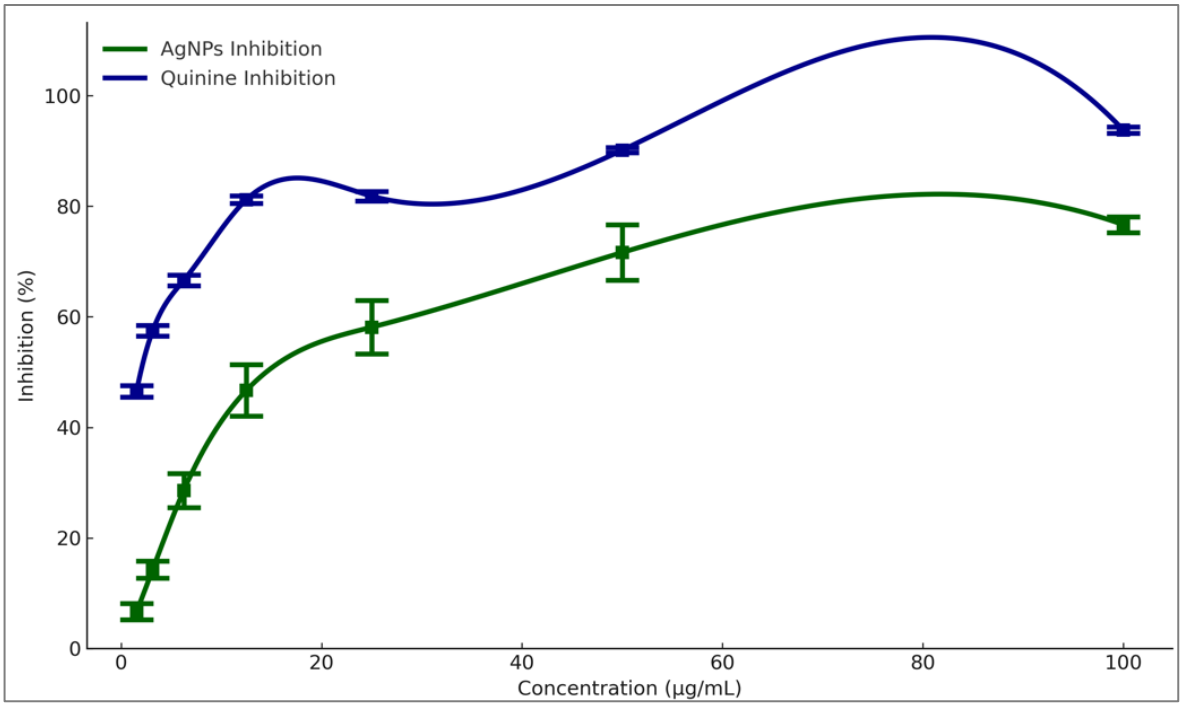

Figure 8: Comparative inhibition profiles of *O. gratissimum*–AgNPs and Quinine.

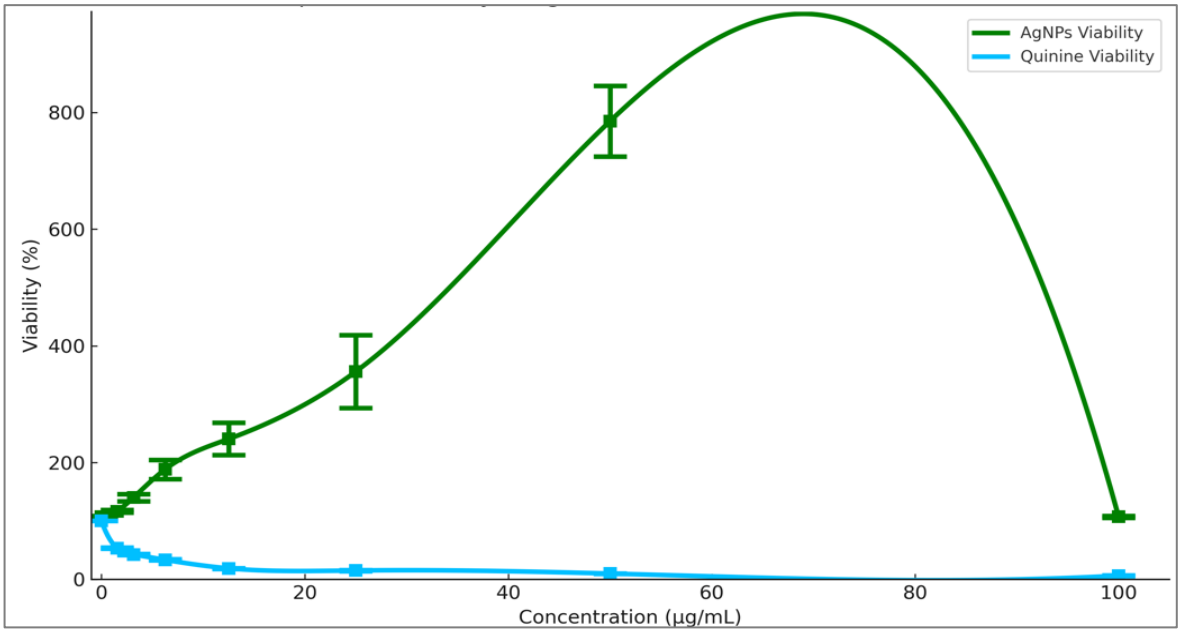

Figure 9: Comparative viability of *O. gratissimum*–AgNPs and Quinine against *P. falciparum*

Table 5: **Antiplasmodial Activity IC_{50} of *O. gratissimum* -AgNPs and Quinine**

Samples	IC50 value (µg/ml)
Plant *(Ocimum gratissimum* -AgNPs*)*	13.70 + 0.99
Control (Quinine)	3.14 + 0.74

Table 6: Comparative Antiplasmodial Activity (IC_{50}) of Green-synthesized AgNPs

Plant Source for AgNP Synthesis	Reported IC_{50} (µg/mL)	Reference
Ocimum gratissimum (This study)	**13.70**	-
Azadirachta indica	15.20	(Bose et al., 2020)
Moringa oleifera	28.50	(Paul et al., 2022)
Terminalia bellirica	9.85	(Singh et al., 2024)
S. tenerrimum	5.42	(Veeragoni et al., 2023)

DISCUSSION

The biosynthesis of silver nanoparticles using *Ocimum gratissimum* leaf extract was successfully optimized for yield and stability. A critical gap in many green synthesis reports is the lack of optimization data, which hinders reproducibility. Our systematic approach varied key parameters, as summarized in Table 1, to establish the optimal conditions for consistent and rapid AgNP formation, indicated by the characteristic color change to dark brown. This visual indicator is a classic signature of the reduction of Ag^+ ions to elemental silver (Ag^0) due to the redox activity of plant phytochemicals (Ahmed et al., 2016). Further characterization provided conclusive evidence of nanoparticle formation, morphology, and composition. Figure 1 and 3 reveals that the synthesized AgNPs were predominantly spherical and well-dispersed with minimal aggregation. This isotropic morphology is a common outcome in plant-mediated synthesis, resulting from the uniform capping and stabilizing action of the phytochemicals present in the extract, which control nucleation and growth (Ibrahim et al., 2025).

The elemental composition via EDX (Figure 2 and Table 2) showed a strong signal for metallic silver, confirming the reduction process. The presence of carbon, oxygen, and nitrogen signals substantiates the presence of an organic capping layer derived from the plant extract, which is crucial for colloidal stability and biocompatibility (Barati et al., 2024). The crystalline nature of the nanoparticles was unequivocally established by XRD analysis (Figure 4). The distinct diffraction peaks at 2θ values of approximately 38.1°, 44.3°, 64.4°, and 77.4° correspond to the (111), (200), (220), and (311) lattice planes of face-centered cubic (fcc) silver, respectively. The intense and sharp nature of the (111) peak suggests a high degree of crystallinity.

The FTIR analysis (Table 3 and Figure 5) identified key functional groups involved in the synthesis. Absorption bands corresponding to C-H stretching (2952.1 cm^{-1}), carbonyl C=O stretching (1796.6 cm^{-1}) from aldehydes/esters, and aromatic N=O stretching (1899.7 cm^{-1}) indicate that compounds such as alkaloids, polyphenols, and terpenoids from *O. gratissimum* are responsible for the reduction of Ag^+ ions and subsequent stabilization of the formed nanoparticles (Bose et al., 2020).

Beyond standard SEM and TEM, we employed Dynamic Light Scattering (DLS) and Zeta potential analysis to provide a holistic view of the nanoparticles' hydrodynamic properties and colloidal stability, addressing a common analytical shortfall in similar studies. The synthesized AgNPs were comprehensively characterized, and their key properties are summarized in Table 4.

The DLS hydrodynamic size (58.3 ± 8.1 nm) was larger than the TEM core size (42.5 ± 5.2 nm), a expected difference due to the hydration layer and the phytochemical corona. The low PDI (0.19) confirms a narrow size distribution. Most notably, the high negative zeta potential of -28.7 mV demonstrates excellent colloidal stability, a crucial factor for consistent biological activity often unreported in similar studies. This stability is imparted by the capping agents, which were identified via FTIR. The novelty of this work is multi-faceted. While a few studies have synthesized AgNPs using *O. gratissimum*, they have primarily focused on antibacterial activity (Egwu et al., 2024; Lawal et al., 2024). This study is among the first to provide a comprehensive *in vitro* assay demonstrated that the *O. gratissimum*-AgNPs possess significant activity against clinical isolate of *P. falciparum*. As detailed in Table 5 and visualized in Figure 8, the inhibitory effect was profoundly concentration-dependent. The percentage inhibition escalated from 6.68% at 1.54 µg/mL to 76.68% at 100 µg/mL, while parasite viability correspondingly plummeted as shown in Figure 7 and Figure 9. This clear dose-response relationship is a hallmark of a specific pharmacologically active agent and confirms the nano-formulation's efficacy in disrupting the parasite's life cycle, particularly schizont development. The calculated IC_{50} value for the *O. gratissimum*-AgNPs was 13.70 ± 0.99 µg/mL. While this is less potent than the standard drug quinine (IC_{50} = 3.14 ± 0.74 µg/mL), Table 6 places this result in direct comparison with other plant-mediated AgNPs, underscoring its competitive potency, it falls within a range considered to represent moderate to good antiplasmodial activity according to established pharmacological criteria (Gardea-Torresdey et al., 2003).

The high antiplasmodial efficacy can be mechanistically attributed to the synergistic interplay between the silver core and the phytochemical cap, enhanced by the optimal physicochemical properties we documented. Size and

Shape. The small size (~42.5 nm) and spherical shape facilitate efficient uptake by infected erythrocytes. Surface Charge: The highly negative zeta potential (-28.7 mV) promotes stability but may also facilitate interaction with positively charged domains on parasite membranes. The primary mechanism involves the release of Ag^+ ions, which generate ROS and inhibit parasite enzymes (glutathione reductase) (Paul et al., 2022). Concurrently, the phytochemical cap (rich in eugenol, thymol) contributes its own antiplasmodial activity, potentially disrupting mitochondrial function and hemoglobin digestion, creating a multi-target "nanobio-hybrid" attack that is less prone to resistance.

CONCLUSION

This study not only successfully synthesizes and characterizes *O. gratissimum*-AgNPs but also addresses critical gaps in the field by providing optimized synthesis parameters, a comprehensive analytical profile (including DLS/Zeta potential), a comparative efficacy benchmark.The demonstrated moderate potency, high selectivity, and excellent stability make these nanoparticles a promising, sustainable candidate for antimalarial therapy. Future work should focus on *in vivo* efficacy studies in a murine model, detailed investigations into the molecular mechanisms of parasite death (apoptosis assays, proteomics), and exploring synergistic interactions with standard antimalarials to combat drug resistance.

REFERENCES

Ahmed, S., Ahmad, M., Swami, B. L., & Ikram, S. (2016). A review on plants extract mediated synthesis of silver nanoparticles for antimicrobial applications: A green expertise. *Journal of Advanced Research, 7*(1), 17–28. [Crossref]

Banerjee, P., Satapathy, M., & Mukhopahayay, A. (2024). Leaf extract mediated green synthesis of silver nanoparticles from seven different Ocimum species: A comparative study on phytochemical composition and antibacterial efficacy. *South African Journal of Botany, 165*, 98–110. [Crossref]

Barati, A., Sahraei, S., Eslami, H., & Sadeghi, F. (2024). Nanotechnology and malaria: Evaluation of efficacy and toxicity of metallic nanoparticles produced by green synthesis. *Journal of Vector Borne Diseases, 61*(3), 221–229. [Crossref]

Bose, S., Mazumdar, D., Banerjee, S., & Chatterjee, S. (2020). Antiplasmodial activity of green synthesized silver nanoparticles using Azadirachta indica leaf extract against Plasmodium falciparum. *Parasitology Research, 119*(8), 2655–2665. [Crossref]

Egwu, I. H., Nwachi, A. C., & Egwu-Ikechukwu, M. M. (2024). Green Synthesis and Antimicrobial Potency of Silver Nanoparticles from Ocimum gratissimum. *Journal of Epidemiological Society of Nigeria, 7*(1-2), 45–53.

Fatima, H. (2024). Antimalarial activity of metallic nanoparticles: Review of earthworm-mediated synthesis and Plasmodium falciparum applications. In *Nanotechnology II* (pp. 403–412). UniqueScientificPublishers. [Link]

Gardea-Torresdey, J. L., Gomez, E., Peralta-Videa, J. R., Parsons, J. G., Troiani, H., & Jose-Yacaman, M. (2003). Alfalfa sprouts: A natural source for the synthesis of silver nanoparticles. *Langmuir, 19*(4), 1357–1361. [Crossref]

Ibrahim, A., & Musa, A. M. (2022). Phytochemical-assisted synthesis of silver nanoparticles: Mechanisms and biomedical potential. *Journal of Applied Nanoscience, 12*(6), 1125–1138. [Crossref]

Ibrahim, A., Muhammad, F.S., Borodo, R.S. & Umar, M. (2025). Ex Vivo Protocol for Evaluating Anti Schizont Activities and Phytochemical Analysis of Zingiber officinale Against Plasmodium falciparum. *Sahel Journal of Life Sciences FUDMA, 3*(1), 384-390. [Crossref]

Iravani, S. (2011). Green synthesis of metal nanoparticles using plants. *Green Chemistry, 13*(10), 2638–2650. [Crossref]

Karthik, L., Kumar, G., Keswani, T., Bhattacharyya, A., Chandar, S. S., & Rao, K. B. (2022). Green synthesis of silver nanoparticles using Coleus amboinicus leaf extract and its application in photocatalytic degradation and antimalarial activity. *Materials Today: Proceedings, 49*, 2663–2669. [Crossref]

Lawal, D., Danjuma, L., & Sani, N. M. (2024). Synthesis, Characterization and Antibacterial Activity of Silver Nanoparticles Synthesized from Ocimum gratissimum Leaf. *African Journal of Pharmaceutical Research and Development, 16*(3), 48–63. [Crossref]

Mela Yoro, J. W. K. J. D. S., Japhet Joshua, Patrick Datheh Bello, Dangiwa Grace Ajima, & Nazifa Umar. (2022). Plant mediated green synthesis, characterization and biological study of silver nanoparticles from Ocimum gratissimum aqueous leaf extract. *Comprehensive Research and Reviews in Chemistry and Pharmacy, 1*(1), 34–40. [Crossref]

Paul, J., Das, S., & Choudhury, S. (2022). Green synthesis of silver nanoparticles from Moringa oleifera leaf extract and their efficacy against Plasmodium falciparum. *Journal of Bionanoscience, 16*(1), 45–52. [Crossref]

Rai, M., Deshmukh, S. D., Ingle, A. P., Gupta, I. R., Galdiero, M., & Galdiero, S. (2021). Metal nanoparticles as a new generation of antimicrobials. *Biotechnology Advances, 53*, 107896. [Crossref]

Rathod, P. K., McErlean, T., & Lee, P. C. (2021). Variations in frequencies of drug-resistant Plasmodium falciparum. *Emerging Infectious Diseases, 27*(3), 870–880. [Crossref]

Salisu, B., Anua, M. S., Wan Ishak, W. R., & Mazlan, N. (2020). Incidence, Distribution and Phenotypic Characterisation of Aflatoxigenic Fungi Contaminating Commonly Consumed Food Grains in Katsina State, Nigeria. *Malaysian Journal of Medicine and Health Sciences, 16*(SUPP11), 2636–9346.

Salisu, B., Anua, M. S., Wan Ishak, W. R., & Mazlan, N. (2022). An improved Fourier-Transform Infrared Spectroscopy combined with partial least squares regression for rapid quantification of total aflatoxins in commercial chicken feeds and food grains. *Journal of Advanced Veterinary and Animal Research, 9*(3), 546–564. [Crossref]

Salisu, B., Anua, M. S., Wan Ishak, W. R., & Mazlan, N. (2024). Bioburden, phenotypic and spectroscopic characterisation of toxigenic and atoxigenic Aspergillus section Flavi from poultry feeds in Kelantan, Malaysia and Katsina, Nigeria. *Malaysian Journal of Microbiology, 20*(2), 120–131. [Crossref]

Salisu, Dandashire, B., Magashi, A. M., Abdulkadir, B., Abbas, M. A., Dauda Goni, M., & Yakubu, A. (2019). Toxicological studies and bioactivity-guided identification of antimicrobially active compounds from crude aqueous stem bark extract of Boswellia dalzielii. *Journal of Advanced Veterinary and Animal Research, 6*(2), 183–192. [Crossref]

Shahzadi, S., Yaqoob, S., Akhtar, S., & Ahmad, R. (2025). A review on green synthesis of silver nanoparticles (SNPs): Focus on biomedical and environmental applications. *RSC Advances, 15*(2), 845–862. [Crossref]

Sharma, A., Sood, K., Kaur, J., & Khatri, M. (2024). Biogenic silver nanoparticles: In-vitro antiplasmodial activity and apoptosis induction in Plasmodium falciparum. *Parasitology International, 98*, 102795. [Crossref]

Singh, S., Mishra, A., Prasad, M., & Shukla, R. (2024). Green-synthesized silver nanoparticles of Terminalia bellirica leaves: Characterization and antimalarial investigation. *BMC Complementary Medicine and Therapies, 24*, Article 123. [Crossref]

Tiwari, S., Sharma, P., Kumar, A., Singh, N., & Rani, M. (2024). Biogenically synthesized green silver nanoparticles exhibit antiplasmodial activity in Plasmodium falciparum (3D7) in vitro. *Nanoscale Research Letters, 19*(1), 242. [Crossref]

Veeragoni, D., Rajendran, R., & Arumugam, P. (2023). In vitro and in vivo antimalarial activity of green-synthesized silver nanoparticles using S. tenerrimum extract. *Acta Tropica, 245*, 106885. [Crossref]

World Health Organization. (2023). *World malaria report 2023*. World Health Organization.